Available online at www.sciencedirect.com
ScienceDirect
Comput. Methods Appl. Mech. Engrg. 294 (2015) 245–258
Computer methods in applied mechanics and engineering
www.elsevier.com/locate/cma

The numerical simulations based on the NND finite difference scheme for shallow water wave equations including sediment concentration☆

Zhendong Luo*, Junqiang Gao

School of Mathematics and Physics, North China Electric Power University, Beijing 102206, China

Received 8 December 2014; received in revised form 11 June 2015; accepted 16 June 2015
Available online 23 June 2015

Abstract

In this study, a numerical model based on the non-oscillatory and non-free parameter dissipation (NND) finite difference scheme for shallow water wave equations including sediment concentration is established in order to simulate the phenomena for dam-break flow and the development of alluvial plain in an estuary. Some numerical experiments show that the numerical model is feasible and efficient for simulating the phenomena for dam-break flow and the development of alluvial plain in an estuary.

MSC: 65M60; 65N30; 65N15

Keywords: Non-oscillatory and non-free parameter dissipation (NND) finite difference scheme; Shallow water wave equations including sediment concentration; Numerical simulation

1. Introduction

A system of shallow water equations (SWEs) can be used to describe the propagation and transformation of short waves in shallow waters, which is also referred to as the Saint-Venant system for one-dimensional case (see [1]). It has extensive applications in ocean, environmental and hydraulic engineering, and coastal engineering, such as the open-channel flows in rivers and reservoirs, the tidal flows in estuary and coastal water regions, the bore wave propagation, the stationary hydraulic jump and river, as mentioned in [2]. Because it is a system of nonlinear partial differential equations, it has no usually analytical solution. One has to rely on numerical solutions.

Many previous studies had explored the numerical solutions for two-dimensional (2D) SWEs that only include the water depth and the velocity of fluid, such as the finite volume (FV) method on unstructured triangular meshes presented by Anatasiou and Chan in [3], the upwind methods established by Bermudez and Vazquez in [4], the parallel

☆ This work is jointly supported by National Science Foundation of China (11271127) and Science Research Project of Guizhou Province Education Department (QJHKYZ[2013]207).
* Corresponding author. Tel.: +86 10 61772167; fax: +86 10 61772167.
E-mail address: zhdluo@ncepu.edu.cn (Z. Luo).

http://dx.doi.org/10.1016/j.cma.2015.06.011
0045-7825/

block preconditioning techniques proposed by Cai and Navon in [5], the optimal control technique of finite element (FE) limited-area addressed by Chen and Navon in [6], the least-squares FE method described by Liang and Hsu in [7], the finite difference (FD) Lax–Wendroff weighted essentially non-oscillatory (WENO) schemes posed by Lu and Qiu in [8], the FE simulation technique of Navon in [9], the FD WENO schemes proposed by Qiu and Shu in [10], the Roes approximate Riemann solver technique of Rogers et al. in [11], the essentially non-oscillatory and WENO schemes with the exact conservation property presented by Vukovic and Sopta in [12], the explicit multi-conservation FD scheme established by Wang in [13], the composite FV method on unstructured meshes proposed by Wang and Liu in [14], the high order FD WENO schemes proposed by Xing and Shu in [15], the high order well-balanced FV WENO schemes and discontinuous Galerkin (DG) methods also proposed by Xing and Shu in [16], the positivity-preserving high order well-balanced DG methods of Xing et al. in [17], the dispersion-correction FD scheme of Yoon et al. in [18], the non-oscillatory FV method given by Yuan and Song in [19], the surface gradient method presented by Zhou et al. in [20], the total variation diminishing FD scheme proposed by Wang et al. in [21], and the high-resolution FVE method established by Vosoughifar et al. in [22].

Compared with the 2D SWEs including only the water depth and the velocity of fluid, the 2D SWEs including sediment concentration have a wider range of applications, which not only can be used to describe the transport and sedimentation of silt and sand in water, the formation and evolution of delta, the expansion of alluvial plain, the migration of rivers, etc., but also can be applied in many real-life applied fields, such as the irrigation systems, the transportation channels, the hydroelectric stations, the ports, and other coastal engineering works. A model for 2D SWES including sediment concentration was established in [23] and has been used more than twenty years in Atmospheric Science and State Key Laboratory of Earth Fluid Dynamics Numerical Simulations at Institute of Atmospheric Physics of Chinese Academy of Sciences. A numerical method based on optimal control approach (see [24]) and a mixed FE formulation (see [25,26]) for the 2D SWEs including sediment concentration are presented. Recently, some numerical simulations was developed (see [27] and here references).

In order to simulate the phenomena for the dam-break flood and the development of the alluvial plain in an estuary, we employ the non-oscillatory and non-free parameter dissipation (NND) technique (see [28]) to establish a numerical model based on the NND FD scheme (NNDFDS) for SWEs including sediment concentration in this study. To the best of our knowledge, there is not any report that the NNDFDS for 2D shallow water equations including sediment concentration has been established, thereby our NNDFDS should be a new method.

The remainder of this article is organized as follows. In Section 2, we establish the numerical model based on NNDFDS for 2D SWEs including sediment concentration. In Section 3, we provide some numerical experiments to show that the numerical model based on NNDFDS is feasible and efficient for simulating the dam-break flood and the development of alluvial plain in an estuary. In Section 4, we provide main conclusions and discussions.

2. Numerical model based on NNDFDS as well as its stability and convergence

2.1. Numerical model based on NNDFDS

Let $\Omega \subset R^2$ be a bounded and connected domain. The governing equations for 2D SWEs including sediment concentration are denoted by the following system of equations (see [23–25])

$$\frac{\partial Z}{\partial t} + \frac{\partial (Zu)}{\partial x} + \frac{\partial (Zv)}{\partial y} = \gamma \left(\frac{\partial^2 Z}{\partial x^2} + \frac{\partial^2 Z}{\partial y^2} \right), \quad (x, y, t) \in \Omega \times (0, T), \tag{1}$$

$$\begin{aligned} &\frac{\partial u}{\partial t} + \frac{\partial (u^2)}{\partial x} + \frac{\partial (vu)}{\partial y} - fv \\ &\quad = A \left(\frac{\partial^2 u}{\partial x^2} + \frac{\partial^2 u}{\partial y^2} \right) - g \frac{\partial (Z + z_b)}{\partial x} - \frac{C_D u \sqrt{u^2 + v^2}}{Z}, \quad (x, y, t) \in \Omega \times (0, T), \end{aligned} \tag{2}$$

$$\begin{aligned} &\frac{\partial v}{\partial t} + \frac{\partial (uv)}{\partial x} + \frac{\partial (v^2)}{\partial y} + fu \\ &\quad = A \left(\frac{\partial^2 v}{\partial x^2} + \frac{\partial^2 v}{\partial y^2} \right) - g \frac{\partial (Z + z_b)}{\partial y} - \frac{C_D v \sqrt{u^2 + v^2}}{Z}, \quad (x, y, t) \in \Omega \times (0, T), \end{aligned} \tag{3}$$

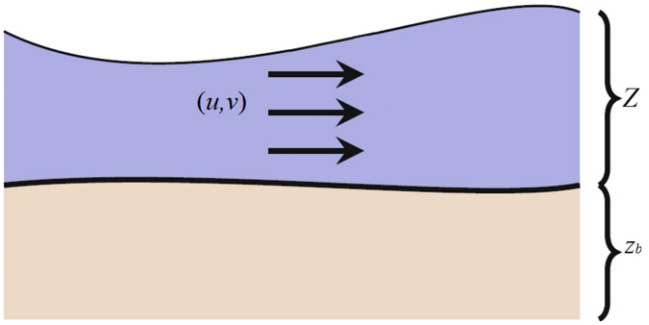

Fig. 1. Water profile.

$$\frac{\partial S}{\partial t}+\frac{\partial(uS)}{\partial x}+\frac{\partial(vS)}{\partial y}=\varepsilon\left(\frac{\partial^2 S}{\partial x^2}+\frac{\partial^2 S}{\partial y^2}\right)+\frac{\alpha\omega(S-S^*)}{Z},\quad (x,y,t)\in\Omega\times(0,T), \tag{4}$$

$$\frac{\partial z_b}{\partial t}+g_b\left(\frac{\partial u}{\partial x}+\frac{\partial v}{\partial y}\right)=\frac{\alpha\omega(S-S^*)}{\rho},\quad (x,y,t)\in\Omega\times(0,T), \tag{5}$$

where γ (m^2/s) and A (m^2/s) are two coefficients of viscosity, (u, v) (m/s) is the vector of velocity, $Z = z - z_b$ (m) is the water depth, z (m) is the surface height, z_b (m) is the height of bed (see Fig. 1), f (1/s) is Coriolis constant, g (m/s^2) is the gravitational constant, C_D (non-dimension) is the coefficient of bottom drag, ε (m^2/s) is the diffusion coefficient of sand, ω (m/s) is the falling speed of suspended sediment particles, S (kg/m^3) is the concentration of sediment in water, ρ (kg/m^3) is the density of dry sand (can be taken as a constant), α (non-dimension) is the constant of variety of sediment, $S^* = K[(u^2+v^2)^{3/2}/(g\omega Z)]^l$ is the capability of sediment transport in bottom bed (is a given empirical function), $g_b = \Gamma(u^2+v^2)^{3/2}Z^p d^q[1-v_c/(u^2+v^2)^{1/2}]$ is also a given empirical function, v_c (m/s) is the velocity of sediment mass transport (is a given function too), d (m) is the diameter of sediment, and K (kg/m^3), l (non-dimension), Γ (s^3/m^2), p (non-dimension), and $q = -p$ are all some empirical constants.

The boundary conditions are supposed to be as follows.

$$\begin{aligned} &Z(x,y,t)=Z_0(x,y,t), \quad u(x,y,t)=u_0(x,y,t), \quad v(x,y,t)=v_0(x,y,t),\\ &S(x,y,t)=S_0(x,y,t), \quad z_b(x,y,t)=z_{b0}(x,y,t), \quad (x,y,t)\in\partial\Omega\times(0,T), \end{aligned} \tag{6}$$

where $Z_0(x, y, t)$, $u_0(x, y, t)$, $v_0(x, y, t)$, $S_0(x, y, t)$, and $z_{b0}(x, y, t)$ are all given functions. The initial conditions are supposed to be as follows.

$$\begin{aligned} &Z(x,y,0)=Z^0(x,y), \quad u(x,y,0)=u^0(x,y), \quad v(x,y,0)=v^0(x,y),\\ &S(x,y,0)=S^0(x,y), \quad z_b(x,y,0)=z_b^0(x,y), \quad (x,y)\in\partial\Omega, \end{aligned} \tag{7}$$

where $Z^0(x, y)$, $u^0(x, y)$, $v^0(x, y)$, $S^0(x, y)$, and $z_b^0(x, y)$ are also given functions.

Let $\triangle t$ be the time step increment, $\triangle x$ and $\triangle y$ denote the spatial step increments, $N = [T/\triangle t]$, $F^r = ru$, $G^r = rv$ $(r = Z, u, v, S)$. By using the NND technique in [28] to discretize (1)–(5), we obtain the numerical model based on NNDFDS for 2D SWEs including sediment concentration as follows:

$$\begin{aligned} \frac{Z_{j,k}^{n+1}-Z_{j,k}^n}{\triangle t} &= \gamma\left(\frac{Z_{j+1,k}^n-2Z_{j,k}^n+Z_{j-1,k}^n}{\triangle x^2}+\frac{Z_{j,k+1}^n-2Z_{j,k}^n+Z_{j,k-1}^n}{\triangle y^2}\right)\\ &\quad-\frac{\bar F_{j+\frac12,k}^{Z,n}-\bar F_{j-\frac12,k}^{Z,n}}{\triangle x}-\frac{\bar G_{j,k+\frac12}^{Z,n}-\bar G_{j,k-\frac12}^{Z,n}}{\triangle y}, \quad n=0,1,2,\ldots,N-1, \end{aligned} \tag{8}$$

$$\begin{aligned}\frac{u_{j,k}^{n+1}-u_{j,k}^{n}}{\triangle t} &= A\left(\frac{u_{j+1,k}^{n}-2u_{j,k}^{n}+u_{j-1,k}^{n}}{\triangle x^2}+\frac{u_{j,k+1}^{n}-2u_{j,k}^{n}+u_{j,k-1}^{n}}{\triangle y^2}\right)\\ &\quad-\frac{\bar{F}_{j+\frac{1}{2},k}^{u,n}-\bar{F}_{j-\frac{1}{2},k}^{u,n}}{\triangle x}-\frac{\bar{G}_{j,k+\frac{1}{2}}^{u,n}-\bar{G}_{j,k-\frac{1}{2}}^{u,n}}{\triangle y}-g\frac{Z_{j+\frac{1}{2},k}^{n}+z_{b,j+\frac{1}{2},k}^{n}-Z_{j-\frac{1}{2},k}^{n}-z_{b,j-\frac{1}{2},k}^{n}}{\triangle x}\\ &\quad+fv_{j,k}^{n}-\frac{C_D u_{j,k}^{n}\sqrt{(u_{j,k}^{n})^2+(v_{j,k}^{n})^2}}{Z_{j,k}^{n}},\quad n=0,1,2,\ldots,N-1,\end{aligned}\tag{9}$$

$$\begin{aligned}\frac{v_{j,k}^{n+1}-v_{j,k}^{n}}{\triangle t} &= A\left(\frac{v_{j+1,k}^{n}-2v_{j,k}^{n}+v_{j-1,k}^{n}}{\triangle x^2}+\frac{v_{j,k+1}^{n}-2v_{j,k}^{n}+v_{j,k-1}^{n}}{\triangle y^2}\right)\\ &\quad-\frac{\bar{F}_{j+\frac{1}{2},k}^{v,n}-\bar{F}_{j-\frac{1}{2},k}^{v,n}}{\triangle x}-\frac{\bar{G}_{j,k+\frac{1}{2}}^{v,n}-\bar{G}_{j,k-\frac{1}{2}}^{v,n}}{\triangle y}-g\frac{Z_{j,k+\frac{1}{2}}^{n}+z_{b,j,k+\frac{1}{2}}^{n}-Z_{j,k-\frac{1}{2}}^{n}-z_{b,j,k-\frac{1}{2}}^{n}}{\triangle y}\\ &\quad-fu_{j,k}^{n}-\frac{C_D v_{j,k}^{n}\sqrt{(u_{j,k}^{n})^2+(v_{j,k}^{n})^2}}{Z_{j,k}^{n}},\quad n=0,1,2,\ldots,N-1,\end{aligned}\tag{10}$$

$$\begin{aligned}\frac{S_{j,k}^{n+1}-S_{j,k}^{n}}{\triangle t} &= \varepsilon\left(\frac{S_{j+1,k}^{n}-2S_{j,k}^{n}+S_{j-1,k}^{n}}{\triangle x^2}+\frac{S_{j,k+1}^{n}-2S_{j,k}^{n}+S_{j,k-1}^{n}}{\triangle y^2}\right)\\ &\quad-\frac{\bar{F}_{j+\frac{1}{2},k}^{S,n}-\bar{F}_{j-\frac{1}{2},k}^{S,n}}{\triangle x}-\frac{\bar{G}_{j,k+\frac{1}{2}}^{S,n}-\bar{G}_{j,k-\frac{1}{2}}^{S,n}}{\triangle y}+\frac{\alpha\omega(S_{j,k}^{n}-S_{j,k}^{*n})}{Z_{j,k}^{n}},\quad n=0,1,2,\ldots,N-1,\end{aligned}\tag{11}$$

$$\begin{aligned}\frac{z_{b,j,k}^{n+1}-z_{b,j,k}^{n}}{\triangle t} &= -\frac{g_{b,j,k}^{n}(u_{j+\frac{1}{2},k}^{n}-u_{j-\frac{1}{2},k}^{n})}{\triangle x}-\frac{g_{b,j,k}^{n}(v_{j,k+\frac{1}{2}}^{n}-v_{j,k-\frac{1}{2}}^{n})}{\triangle y}\\ &\quad+\frac{\alpha\omega(S_{j,k}^{n}-S_{j,k}^{*n})}{\rho},\quad n=0,1,2,\ldots,N-1,\end{aligned}\tag{12}$$

where

$$\bar{F}_{j+\frac{1}{2},k}^{r,n}=F_{j+\frac{1}{2},k,L}^{r,n,+}+F_{j+\frac{1}{2},k,R}^{r,n,-},$$

$$F_{j+\frac{1}{2},k,L}^{r,n,+}=F_{j,k}^{r,n,+}+\frac{1}{2}\text{minmod}(\triangle F_{j-\frac{1}{2},k}^{r,n,+},\triangle F_{j+\frac{1}{2},k}^{r,n,+}),$$

$$F_{j+\frac{1}{2},k,R}^{r,n,-}=F_{j+1,k}^{r,n,-}-\frac{1}{2}\text{minmod}(\triangle F_{j+\frac{1}{2},k}^{r,n,-},\triangle F_{j+\frac{3}{2},k}^{r,n,-}),$$

$$\triangle F_{j+\frac{1}{2},k}^{r,n,\pm}=F_{j+1,k}^{r,n,\pm}-F_{j,k}^{r,n,\pm},$$

$$\bar{G}_{j,k+\frac{1}{2}}^{r,n}=G_{j,k+\frac{1}{2},B}^{r,n,+}+G_{j,k+\frac{1}{2},T}^{r,n,-},$$

$$G_{j,k+\frac{1}{2},B}^{r,n,+}=G_{j,k}^{r,n,+}+\frac{1}{2}\text{minmod}(\triangle G_{j,k-\frac{1}{2}}^{r,n,+},\triangle G_{j,k+\frac{1}{2}}^{r,n,+}),$$

$$G_{j,k+\frac{1}{2},T}^{r,n,-}=G_{j,k+1}^{r,n,-}-\frac{1}{2}\text{minmod}(\triangle G_{j,k+\frac{1}{2}}^{r,n,-},\triangle G_{j,k+\frac{3}{2}}^{r,n,-}),$$

$$\triangle G_{j,k+\frac{1}{2}}^{r,n,\pm}=G_{j,k+1}^{r,n,\pm}-G_{j,k}^{r,n,\pm},$$

$$\text{minmod}(a,b)=\begin{cases}\min(|a|,|b|), & a>0 \text{ and } b>0,\\ -\min(|a|,|b|), & a<0 \text{ and } b<0,\\ 0, & a\cdot b\leqslant 0,\end{cases}$$

$$a^{+}(x,y,t)=\begin{cases}a(x,y,t), & a(x,y,t)\geqslant 0,\\ 0, & a(x,y,t)<0,\end{cases}$$

$$a^-(x,y,t) = -\begin{cases} a(x,y,t), & a(x,y,t) \leqslant 0, \\ 0, & a(x,y,t) > 0. \end{cases}$$

2.2. Stability and convergence of sequence of solutions for NNDFDS

In order to prove the local stability and convergence of sequence of solutions for NNDFDS (8)–(12), it is necessary to introduce the following discrete Gronwall Lemma (see [26]).

Lemma 2.1. *If $\{a_n\}$, $\{b_n\}$, and $\{c_n\}$ are three positive sequences, and $\{c_n\}$ is monotone, that satisfy $a_0 + b_0 \leqslant c_0$ and $a_n + b_n \leqslant c_n + \bar{\lambda}\sum_{i=0}^{n-1} a_i$ $(\bar{\lambda} > 0, n = 1, 2, \ldots)$, then $a_n + b_n \leqslant c_n \exp(n\bar{\lambda})$ $(n = 0, 1, 2, \ldots)$.*

In the following, by using the stability analysis technique of FD schemes (see [29] or [30]), we provide the proof of local stability and convergence for NNDFDS (8)–(12).

Theorem 2.2. *Under the conditions $\triangle t \cdot (|u| + |v|) \leqslant \min\{4\gamma, 4\varepsilon, 4A\}$ and $4\triangle t \max\{\gamma, A, \varepsilon\} \leqslant \min\{\triangle x^2, \triangle y^2\}$, the NNDFDS (8)–(12) is locally stable. Further, the sequence of solutions for the NNDFDS (8)–(12) is convergent and has the following error estimates*

$$|r(x_j, y_k, t_n) - r^n_{j,k}| = O(\Delta t, \Delta x^2, \Delta y^2), \quad 1 \leqslant n \leqslant N, 1 \leqslant j \leqslant J, 1 \leqslant k \leqslant K, r = Z, u, v, S, z_b, \tag{13}$$

where $J = \max_{(x_1,y),(x_2,y)\in\Omega} |x_1 - x_2|$, and $K = \max_{(x,y_1),(x,y_2)\in\Omega} |y_1 - y_2|$.

Proof. If $4\triangle t \max\{\gamma, A, \varepsilon\} \leqslant \min\{\triangle x^2, \triangle y^2\}$ and $\triangle t \cdot (|u| + |v|) \leqslant \min\{4\gamma, 4\varepsilon, 4A\}$, which implies $\gamma\triangle t/\triangle x^2 \leqslant 1/4$ and $\gamma\triangle t/\triangle y^2 \leqslant 1/4$ as well as $4\triangle t(\|u\|_\infty + \|v\|_\infty) \leqslant \min\{\gamma, \varepsilon, A\}$, by (8), we have

$$\begin{aligned} |Z^{n+1}_{j,k}| &\leqslant \left(1 - \frac{2\gamma\triangle t}{\triangle x^2} - \frac{2\gamma\triangle t}{\triangle y^2}\right)|Z^n_{j,k}| + \frac{\gamma\triangle t}{\triangle x^2}(|Z^n_{j+1,k}| + |Z^n_{j-1,k}|) + \frac{\gamma\triangle t}{\triangle y^2}(|Z^n_{j,k+1}| + |Z^n_{j,k-1}|) \\ &\quad + \frac{\triangle t}{\triangle x}(|\bar{F}^{Z,n}_{j+\frac{1}{2},k}| + |\bar{F}^{Z,n}_{j-\frac{1}{2},k}|) + \frac{\triangle t}{\triangle y}(|\bar{G}^{Z,n}_{j,k+\frac{1}{2}}| + |\bar{G}^{Z,n}_{j,k-\frac{1}{2}}|) \\ &\leqslant \left(1 + \frac{2\triangle t}{\triangle x}\|u\|_\infty + \frac{2\triangle t}{\triangle y}\|v\|_\infty\right)\|Z^n\|_\infty \leqslant \left(1 + \frac{\gamma}{2\triangle x} + \frac{\gamma}{2\triangle y}\right)\|Z^n\|_\infty, \end{aligned} \tag{14}$$

where $\|\cdot\|_\infty$ is the norm in $L^\infty(\Omega)$. Thus, from (14), we obtain

$$\|Z^{n+1}\|_\infty \leqslant \left(1 + \frac{\gamma}{2\triangle x} + \frac{\gamma}{2\triangle y}\right)\|Z^n\|_\infty, \quad n = 0, 1, 2, \ldots, N-1. \tag{15}$$

Summing (15) from 0 to n yields

$$\|Z^{n+1}\|_\infty \leqslant \|Z^0\|_\infty + \left(\frac{\gamma}{2\triangle x} + \frac{\gamma}{2\triangle y}\right)\sum_{j=0}^{n}\|Z^n\|_\infty, \quad n = 0, 1, 2, \ldots, N-1. \tag{16}$$

By applying Discrete Gronwall Lemma 2.1 to (16), we obtain

$$\|Z^{n+1}\|_\infty \leqslant \|Z^0\|_\infty \exp\left(\frac{n\gamma}{2\triangle x} + \frac{n\gamma}{2\triangle y}\right), \quad n = 0, 1, 2, \ldots, N-1, \tag{17}$$

which shows that the series $\{Z^{n+1}\}$ is local stable when the time interval $[0, T]$ is finite. Further, it is convergent from Lax's theorem of stability (see [29] or [30]). The water depth is positive, so there are two positive constants β_1 and β_2 such that

$$\beta_1 \leqslant \|Z^n\|_\infty \leqslant \beta_2, \quad n = 0, 1, 2, \ldots, N. \tag{18}$$

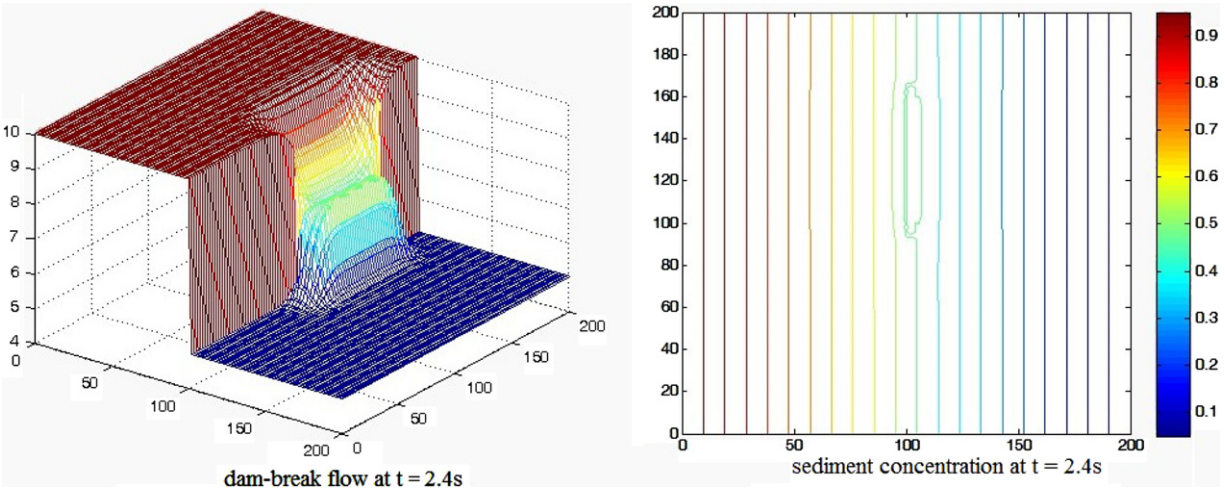

Fig. 2. The status of dam-break flow and sediment concentration at $t = 2.4$ s, respectively.

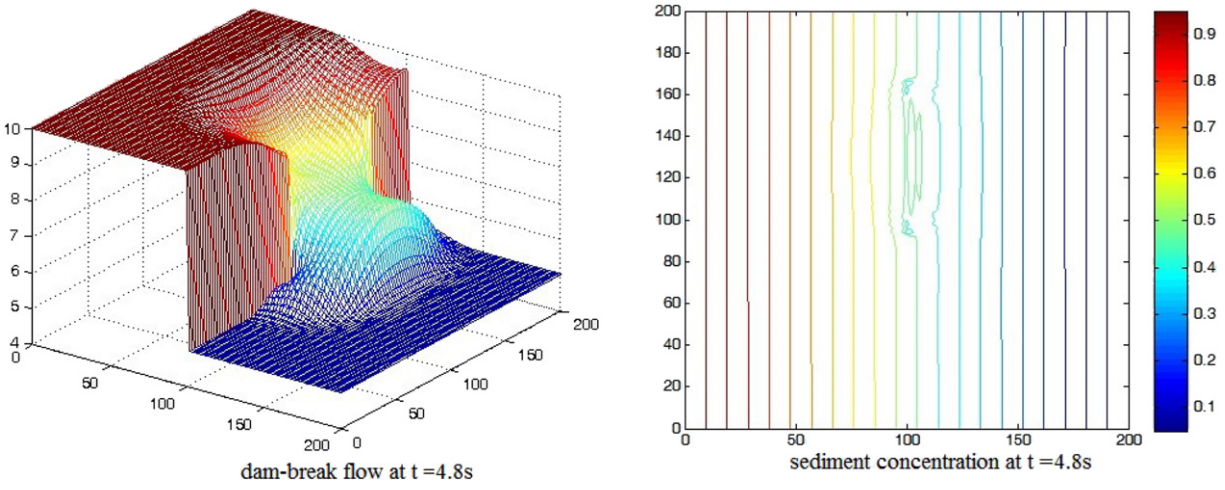

Fig. 3. The status of dam-break flow and sediment concentration at $t = 4.8$ s, respectively.

If $\triangle t \cdot (|u| + |v|) \leqslant \min\{4\gamma, 4\varepsilon, 4A\}$ and $4\triangle t \max\{\gamma, A, \varepsilon\} \leqslant \min\{\triangle x^2, \triangle y^2\}$, then by using the same approach used to prove (15), by (18) and from (9)–(12), we obtain

$$\|u^{n+1}\|_\infty \leqslant \left(1 + \frac{A}{2\triangle x} + \frac{A}{2\triangle y}\right)\|u^n\|_\infty + \frac{2g\triangle t}{\triangle x}\|Z^n\|_\infty + \frac{2g\triangle t}{\triangle x}\|z_b^n\|_\infty + \triangle t|f|\|v^n\|_\infty + \frac{C_D A}{4\beta_1}(\|u^n\|_\infty + \|v^n\|_\infty), \quad n = 0, 1, 2, \ldots, N, \tag{19}$$

$$\|v^{n+1}\|_\infty \leqslant \left(1 + \frac{A}{2\triangle x} + \frac{A}{2\triangle y}\right)\|v^n\|_\infty + \frac{2g\triangle t}{\triangle y}\|Z^n\|_\infty + \frac{2g\triangle t}{\triangle y}\|z_b^n\|_\infty + \triangle t|f|\|u^n\|_\infty + \frac{C_D A}{4\beta_1}(\|u^n\|_\infty + \|v^n\|_\infty), \quad n = 0, 1, 2, \ldots, N, \tag{20}$$

$$\|S^{n+1}\|_\infty \leqslant \left(1 + \frac{\varepsilon}{2\triangle x} + \frac{\varepsilon}{2\triangle y}\right)\|S^n\|_\infty + \frac{\alpha\omega\triangle t}{\beta_1}(\|S^n\|_\infty + \|S^{*n}\|_\infty), \quad n = 0, 1, 2, \ldots, N, \tag{21}$$

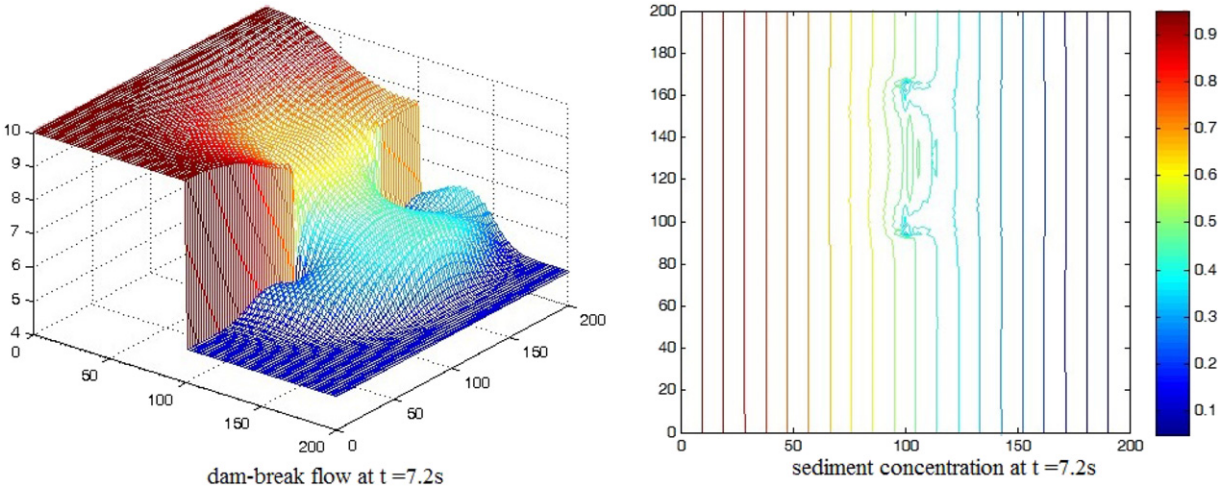

Fig. 4. The status of dam-break flow and sediment concentration at $t = 7.2$ s, respectively.

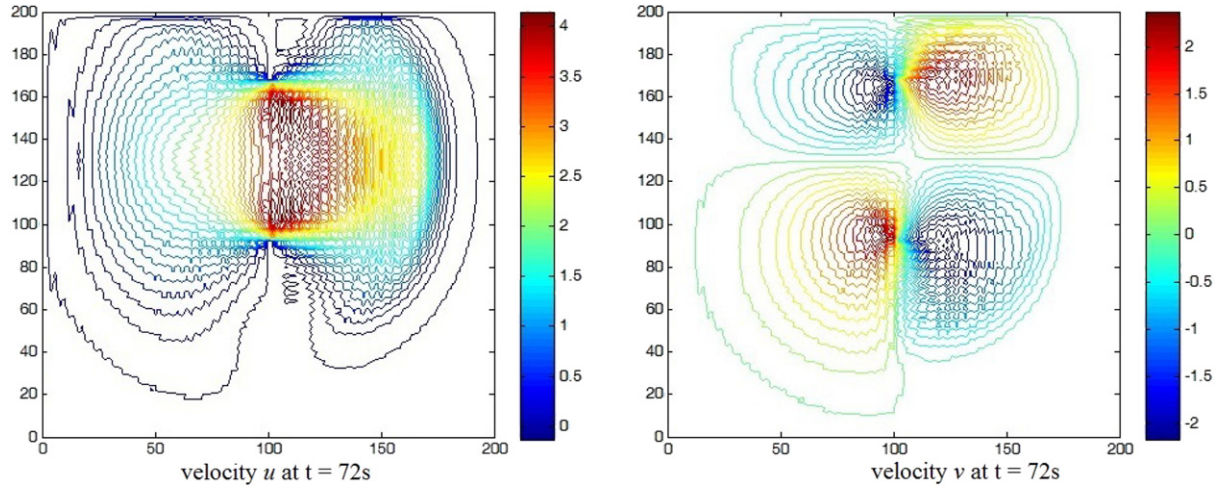

Fig. 5. The status of velocity in x- and y-directions at $t = 7.2$ s, respectively.

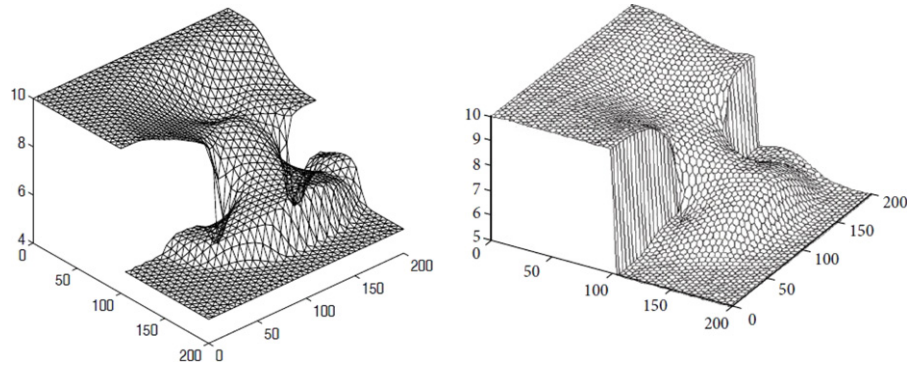

Fig. 6. The left and right charts are the FVE solutions of the dam-break flow in [19] and [23] at $t = 7.2$ s, respectively.

$$\|z_b^{n+1}\|_\infty \leqslant 2\triangle t\|g_b^n\|_\infty\left(\frac{\|u^n\|_\infty}{\triangle x}+\frac{\|v^n\|_\infty}{\triangle y}\right)+\frac{\alpha\omega\triangle t}{\rho}(\|S^n\|_\infty+\|S^{*n}\|_\infty),\quad n=0,1,2,\ldots,N. \tag{22}$$

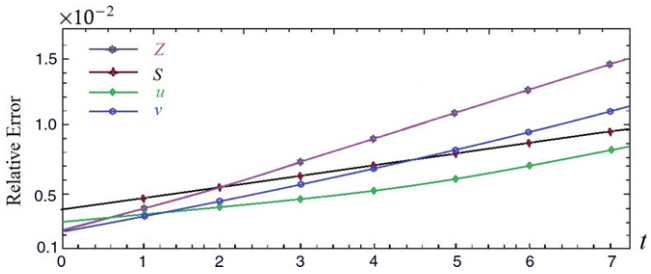

Fig. 7. The changes of relative errors of NNDFDS solutions of velocity, sediment concentration, and water depth of the dam-break flow on [0, 7.2] s.

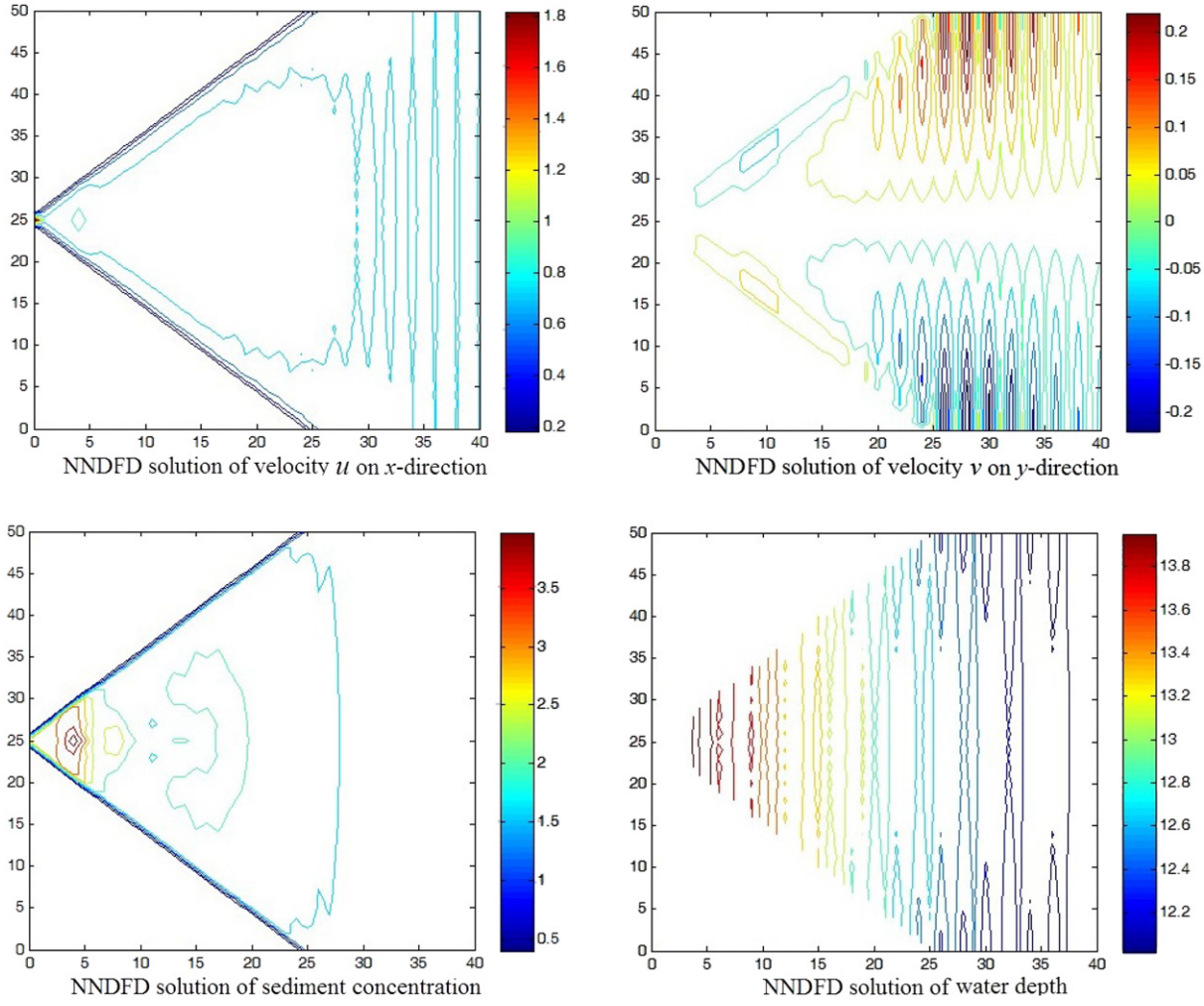

Fig. 8. The status of velocity, sediment concentration, and water depth in the delta of an estuary in the third month.

Note that

$$\begin{aligned}\|S^{*n}\|_\infty &\leqslant K[(\|u^n\|_\infty^2+\|v^n\|_\infty^2)^{3/2}/(g\omega\beta_1)]^l\\ &\leqslant K[(A/\Delta t)^{2l}/(g\omega\beta_1)^l](\|u^n\|_\infty+\|v^n\|_\infty),\\ \|g_b^n\|_\infty &\leqslant \Gamma\beta_2^p d^q(\|u^n\|_\infty^2+\|v^n\|_\infty^2)^{3/2}\leqslant \Gamma\beta_2^p d^q(A/\Delta t)^3.\end{aligned}$$

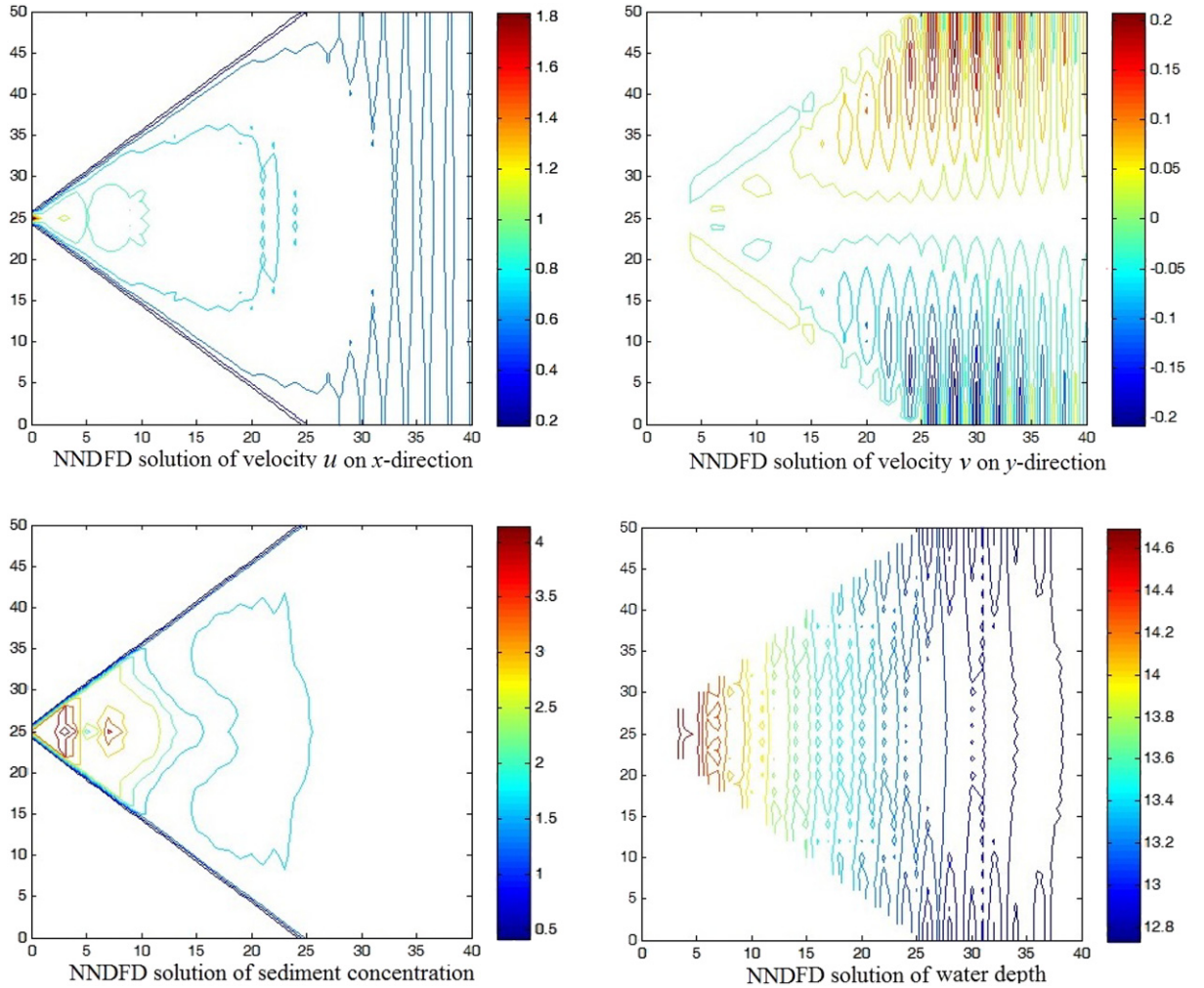

Fig. 9. The status of velocity, sediment concentration, and water depth in the delta of an estuary in the first year.

Put $\varpi = \max\{K[(A/\triangle t)^{2l}/(g\omega\beta_1)^l]\alpha\omega\triangle t/(\beta_1+\rho) + A/(2\triangle x + 2\triangle y) + \triangle t|f| + 2C_DA/(4\beta_1) + 2\Gamma\beta_2^p d^q A^3/(\triangle x\triangle t^2), 2g\triangle t/(\triangle x+\triangle y) + K[(A/\triangle t)^{2l}/(g\omega\beta_1)^l]\alpha\omega\triangle t/(\beta_1+\rho), A/(2\triangle x + \triangle t|f| + 2\triangle y) + 2\Gamma\beta_2^p d^q A^3/(\triangle y\triangle t^2) + 2C_DA/(4\beta_1), \varepsilon/(2\triangle x) + \varepsilon/(2\triangle y) + \alpha\omega\triangle t/(\beta_1+\rho)\}$. From (19)–(22), we obtain

$$\|u^{n+1}\|_\infty + \|v^{n+1}\|_\infty + \|S^{n+1}\|_\infty + \|z_b^{n+1}\|_\infty \leqslant (1+\varpi)(\|u^n\|_\infty + \|v^n\|_\infty + \|S^n\|_\infty + \|z_b^n\|_\infty) + \left(\frac{2g\triangle t}{\triangle x} + \frac{2g\triangle t}{\triangle y}\right)\|Z^0\|_\infty \exp\left(\frac{n\gamma}{2\triangle x} + \frac{n\gamma}{2\triangle y}\right), \quad n = 0, 1, 2, \ldots, N. \tag{23}$$

Summing (23) from 0 to n and using Lemma 2.1 yield that

$$\|u^{n+1}\|_\infty + \|v^{n+1}\|_\infty + \|S^{n+1}\|_\infty + \|z_b^{n+1}\|_\infty \leqslant (\|u^0\|_\infty + \|v^0\|_\infty + \|S^0\|_\infty + \|z_b^0\|_\infty)\exp(n\varpi) + \left(\frac{2gn\triangle t}{\triangle x} + \frac{2gn\triangle t}{\triangle y}\right)\|Z^0\|_\infty \exp\left(\frac{n\gamma}{2\triangle x} + \frac{n\gamma}{2\triangle y}\right)\exp(n\varpi), \quad n = 0, 1, 2, \ldots, N. \tag{24}$$

When the time interval $[0, T]$ is finite, the right hand side of (24) is bounded. Thus, we conclude that the sequence $\{u^n, v^n, S^n, z_b^n\}$ is locally stable. Further, with Lax's theorem of stability (see [30] or [22]), we conclude that the sequence of solutions for the NNDFDS (8)–(12) is convergent. By means of Taylor's formula to expand (8)–(12) at reference point (x_j, y_k, t_n), we could easily obtain the error estimates (13), which completes the proof of Theorem 2.2. □

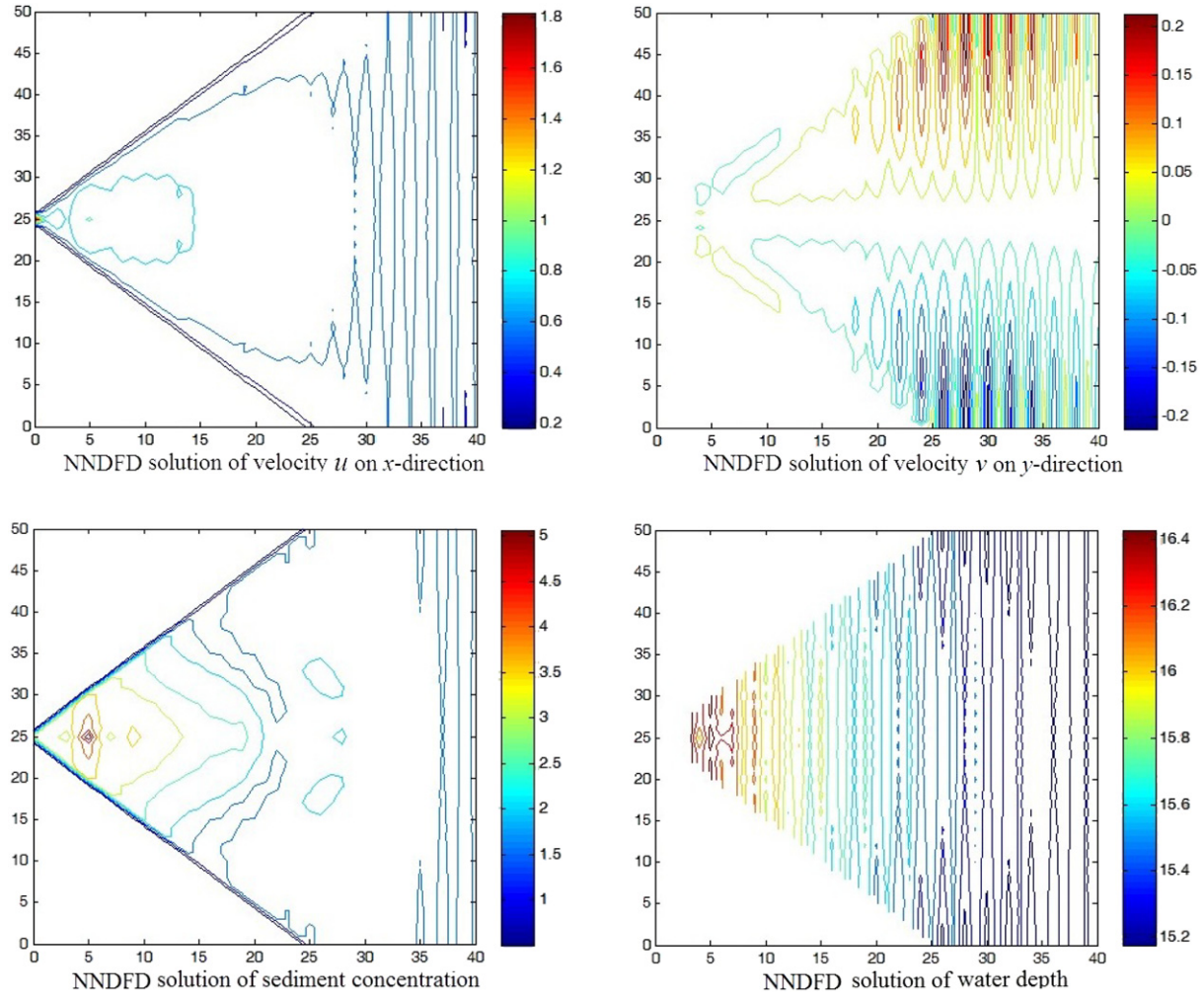

Fig. 10. The status of velocity, sediment concentration, and water depth in the delta of an estuary in the third year.

Remark 2.3. The NNDFDS (8)–(12) is only first-order approximate accuracy in time. If one wants to achieve higher order time approximate accuracy, it is necessary to change the time difference quotients on the left hand sides in (8)–(12) into higher order ones (e.g., time central difference quotients or time second-order difference quotients). Because the numerical model (8)–(12) adopts NND technique, it can capture shock wave very well (see the numerical experiments in Section 3).

3. Numerical experiments

In this section, we present two numerical experiments that demonstrate the feasibility and efficiency of the numerical model (8)–(12) based on NNDFDS for 2D SWEs including sediment concentration.

3.1. Example for simulating dam-break flow

A dam-break flow is an uncontrolled release of water when a vertical barrier is suddenly removed and it is the simplest available model for a lot of important phenomena, such as break-out floods, sheet flow events and the formative stages of lahars or debris flows.

An idealized model of the dam-break flow may show that the barrier at $x = 100$ and $0 \leqslant y \leqslant 200$ divides fluids of different depths 10 m and 5 m, until time $t = 0$, when a gate of width 75 m (i.e., on $x = 100$ and $95 \leqslant y \leqslant 170$)

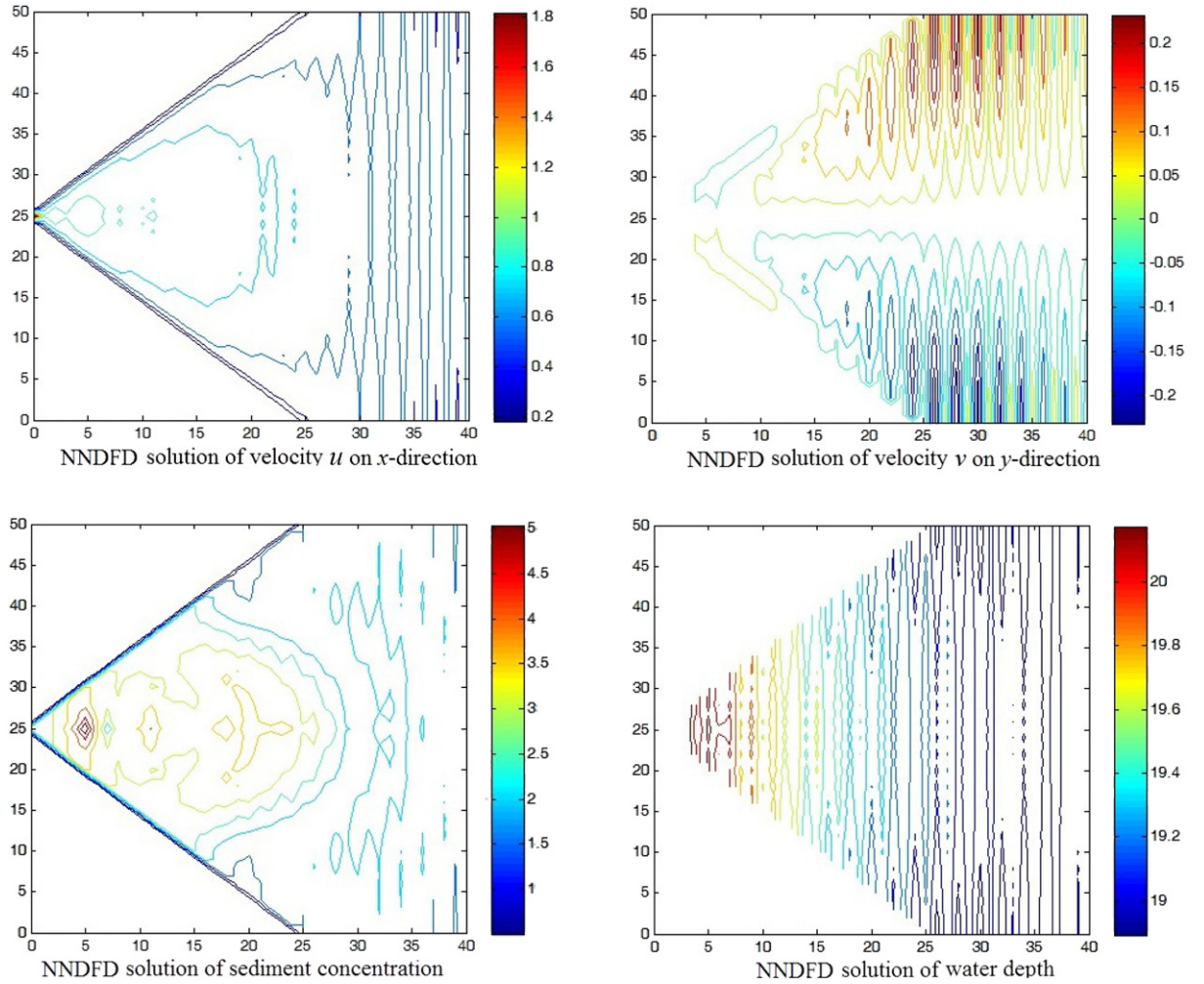

Fig. 11. The status of velocity, sediment concentration, and water depth in the delta of an estuary in the fifth year.

in the barrier is instantaneously removed and fluid (depth 10 m) floods into the shallower region (depth 5 m). Thus, the computational domain for dam-break flow is a square of area 200×200 m^2, i.e., $\bar{\Omega} = [0,\ 200] \times [0,\ 200]$, which holds the water depths 10 m on sub-domain $[0,\ 100] \times [0,\ 200]$ and 5 m on sub-domain $[100,\ 200] \times [0,\ 200]$, respectively. Since $z_b = 0$, thus, $z^n_{b,j,k} = 0$ in (8)–(12).

In order to simulate the dam-break flow by means of the NNDFDS (8)–(12) of 2D SWEs including sediment concentration, it is necessary to take the time step $\Delta t = 0.01$ s and the spatial step $\Delta x = \Delta y = 0.02$ m and to designate all of parameters: $f = 1.1 \times 10^{-4}$, $\gamma = 0.001$, $A = 7.5 \times 10^{-3}$, $C_D = 0.01$, $\omega = 0.01$, $\alpha = 0.3$, $K = 0.35$, $l = 0.92$, and $\rho = 1.5 \times 10^3$ (see [19,23]).

By means of the NNDFDS (8)–(12), we obtain the NNDFD solutions of dam-break flow and sediment concentration ($z_b = 0$, so it is not described) when $n = 240$, 480, and 720 (i.e., at 2.4 s, 4.8 s, and 7.2 s), as shown in the left and right columns in Figs. 2–4, respectively. We also obtained the NNDFD solutions of velocity u and v in x- and y-directions at $t = 7.2$ s, as shown in left and right charts in Fig. 5, respectively.

We compared the NNDFDS solution at $t = 7.2$ s of dam-break flow in the left chart in Fig. 4 with the FVE solution in [19] in the left chart and the high-resolution FVE solution in [22] in the right chart in Fig. 6, respectively, where we found that the FVE solution in [19] had obvious oscillatory and dispersion, and the high-resolution FVE solution in [22] has also obvious oscillatory and dissipation, whereas the current NNDFDS solution of dam-break flow in the left chart in Fig. 4 had no oscillatory, dispersion, and dissipation. Especially, our NNDFDS could simultaneously simulate the status of dam-break flow and sediment concentration. Therefore, we showed that the current NNDFDS

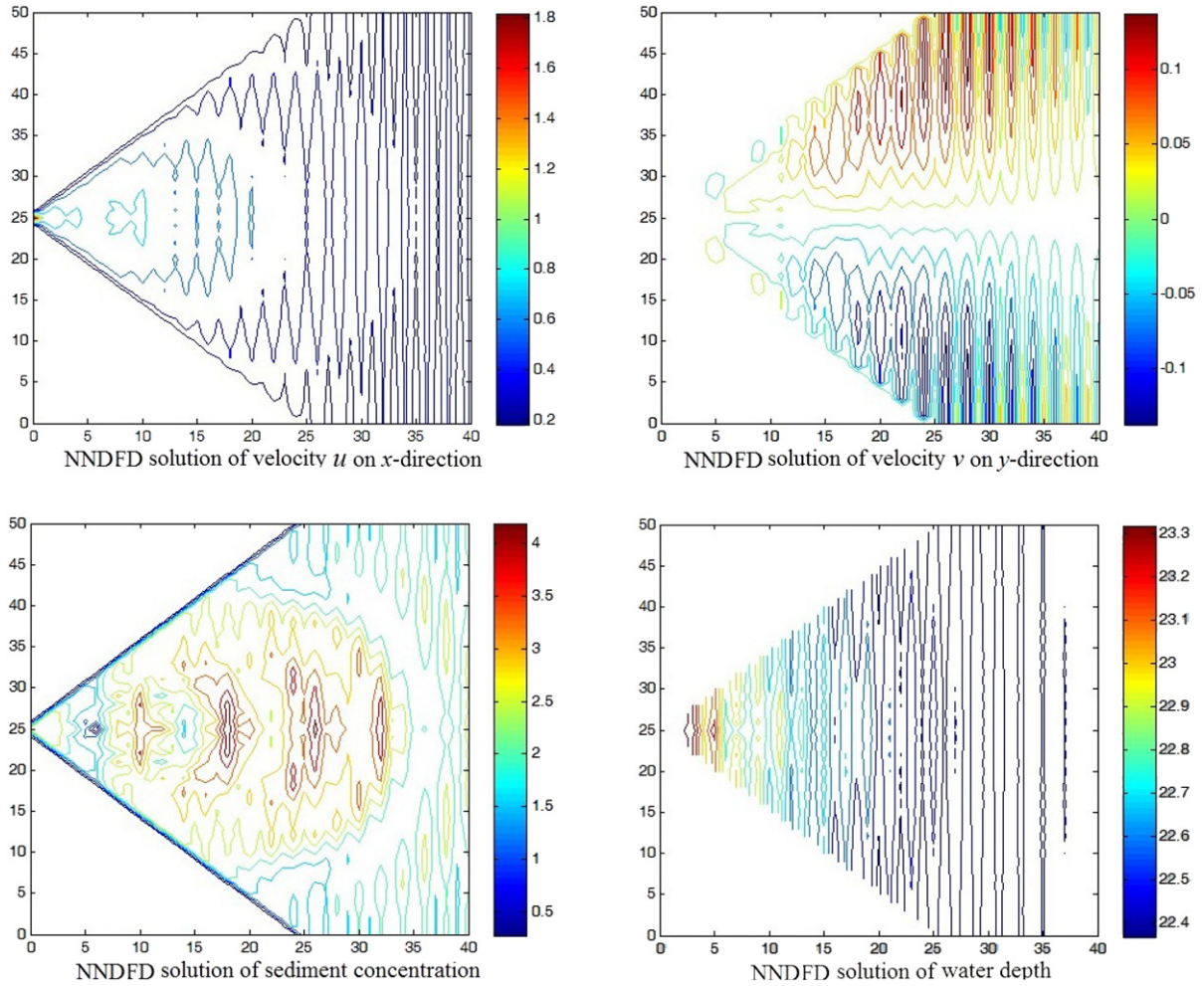

Fig. 12. The status of velocity, sediment concentration, and water depth in the delta of an estuary in the ninth year.

was far better than those in [9] and [22]. We also showed that the NNDFDS (8)–(12) was really one of the existing best numerical methods and was very feasible and efficient for simulating the dam-break flow.

Fig. 7 shows the relative errors of the velocities in x- and y-directions, the sediment concentration, and the water depth of the dam-break flow on $[0, 7.2]$ s, which is computed by the formulas $(u^{n+1} - u^n)/u^n$, $(v^{n+1} - v^n)/v^n$, $(S^{n+1} - S^n)/S^n$, and $(Z^{n+1} - Z^n)/Z^n$, respectively. We computed from Theorem 2.2 that the theoretical error was $O(\Delta t, \Delta x^2, \Delta y^2) = O(10^{-2})$, whereas the relative errors of the numerical solutions were also $O(10^{-2})$, so the relative errors of the numerical solutions were consistent with theoretical error.

3.2. *Example for simulating sediment transport and flow in an estuary*

The computational domain is $\bar{\Omega} = \{(x, y) : 23 - 23x/25 \leqslant y \leqslant 27 + 33x/25, 0 \leqslant x \leqslant 25\} \cup \{(x, y) : 25 \leqslant x \leqslant 40, 0 \leqslant y \leqslant 50\}$ (the unit of x and y is km). The depth at entrance is 10 m (i.e., $Z_0|_{x=0} = 0.01$ km). The sediment thickness at entrance is 2 m (i.e., $z_{b0}|_{x=0} = 0.002$ km). The velocity u_0 of fluid in x-direction from the entrance is 2 m/s (i.e., $u_0|_{x=0} = 7.2$ km/h), but $v_0 = 0$. The sediment concentration in water flow is 1.2 kg/m^3 (i.e., $S_0 = S^0 = 1.2 \times 10^{-3}$ kg/km^3). The change in bottom topography every 100 km falls 1 m along the flow direction (i.e., $z_{b0} = z_b^0 = 10^{-5}x + 2, 0 \leqslant x \leqslant 40$). The bilateral boundaries of the water flow are two solid borders, i.e., $u_0 = v_0 = 0$ on set $\{(x, y) : y = 23 - 23x/25, 0 \leqslant x \leqslant 25\} \cup \{(x, y) : y = 27 + 33x/25, 0 \leqslant x \leqslant 25\} \cup \{(x, 0) : 25 \leqslant x \leqslant 40\} \cup \{(x, 50) : 25 \leqslant x \leqslant 40\}$. The time step $\Delta t = 3600$ s $= 1$ h. The spatial step

$\Delta x = \Delta y = 200\ \text{m} = 0.2\ \text{km}$. According to [23], we take $f = 1.1 \times 10^{-4}$, $\gamma = 0.001$, $A = 7.5 \times 10^{-3}$, $C_D = 0.01$, $d = 0.001$, $\omega = 0.01$, $v_c = 0$, $\alpha = 0.3$, $K = 0.35$, $\Gamma = 5$, $r = 0.92$, $n = 3$, $p = -0.25$, $q = 0.25$, and $\rho = 1.5 \times 10^3$.

By means of the NNDFDS (8)–(12), we obtained the NNDFD solutions $u^n_{j+\frac{1}{2},k}$ and $v^n_{j,k+\frac{1}{2}}$, $S^n_{j,k}$, and $Z^n_{j,k}$ for the velocity u in x-direction and v in y-direction, the sediment concentration S, and the water depth Z (the change of z_b was very small, so it is not described) when $n = 2160$, 8760, 26,280, 43,800, and 78,840 (i.e., in the third month, first year, third year, fifth year, and ninth year), which are depicted graphically in the charts in Figs. 8, 9, 10, 11, and 12, respectively. We exhibited that these numerical results had really shown the status of sediment transport and the development of alluvial plain in an estuary. Especially, the numerical solutions on very long time was still convergent and stable. We also showed that the numerical model (8)–(12) based on NNDFDS for 2D SWEs including sediment concentration was very feasible and efficient for simulating sediment transport and flow in an estuary.

4. Conclusions and discussions

In the current research, we established the numerical model based on NNDFDS for 2D SWEs including sediment concentration. We presented two numerical examples to illustrate that the numerical model based on NNDFDS is very effective for finding the numerical solutions of SWEs including sediment concentration. The numerical model based on NNDFDS can capture shock wave better than previous methods such as the numerical models in [19,22] and can also simulate the status of sediment transport and the development of alluvial plain in an estuary. Especially, the numerical model based on NNDFDS for 2D SWEs including sediment concentration is completely different from existing numerical models for SWEs (see, e.g., [3–22,27]) and is an improvement and development for these existing numerical models.

Future research work in this area will aim at extending the NNDFDS, applying it to simulating more real-life problems such as the tidal flows in an estuary and coastal water regions, the bore wave propagation, and the stationary hydraulic jump and river.

Acknowledgments

The authors of this article thank the reviewers and editors very much for their valuable suggestions.

References

[1] A.J.C. de Saint-Venant, Théorie du mouvement non permanent des eaux, avec application aux crues des rivirres et à l'introduction des marées dans leur lit, C. R. Acad. Sci. Paris 73 (1871) 147–154.
[2] V. Giovangigli, B. Tran, Mathematical analysis of a Saint-Venant model with variable temperature, Math. Models Methods Appl. Sci. 20 (8) (2010) 1251–1297.
[3] K. Anatasiou, C.T. Chan, Solution of the 2d shallow water equations using the finite volume method on unstructures triangular meshes, Internat. J. Numer. Methods Fluids 24 (1997) 1225–1245.
[4] A. Bermudez, M.E. Vazquez, Upwind methods for hyperbolic conservation laws with source terms, Comput. Fluids 23 (1994) 1049–1071.
[5] Y. Cai, I.M. Navon, Parallel block preconditioning techniques for the numerical simulation of the shallow water flow using finite element methods, J. Comput. Phys. 122 (1995) 39–50.
[6] X. Chen, I.M. Navon, Optimal control of a finite-element limited-area shallow-water equations model, Stud. Inf. Control 18 (1) (2009) 41–62.
[7] A.J. Liang, T.W. Hsu, Least-squares finite-element method for shallow-water equations with source terms, Acta Mech. Sin. 25 (2009) 597–610.
[8] C.N. Lu, J.X. Qiu, Simulations of shallow water equations with finite difference Lax–Wendroff weighted essentially non-oscillatory schemes, J. Sci. Comput. 47 (3) (2011) 281–302.
[9] I.M. Navon, Finite-element simulation of the shallow-water equations model on a limited area domain, Appl. Math. Model. 3 (1) (1979) 337–348.
[10] J.X. Qiu, C.W. Shu, Finite difference WENO schemes with Lax–Wendroff-type time discretizations, SIAM J. Sci. Comput. 24 (2003) 2185–2198.
[11] B.D. Rogers, A.G.L. Borthwick, P.H. Taylor, Mathematical balancing of flux gradient and source terms prior to using Roe's approximate Riemann solver, J. Comput. Phys. 192 (2003) 422–451.
[12] S. Vukovic, L. Sopta, ENO and WENO schemes with the exact conservation property for one dimensional shallow water equations, J. Comput. Phys. 179 (2002) 593–621.
[13] B. Wang, An explicit multi-conservation finite-difference scheme for shallow-water-wave equation, J. Comput. Math. 26 (3) (2008) 404–409.
[14] J.S. Wang, R.X. Liu, The composite finite volume method on unstructured meshes for 2D shallow water equations, Internat. J. Numer. Methods Fluids 37 (2001) 933–949.
[15] Y. Xing, C.W. Shu, High order finite difference WENO schemes with the exact conservation property for the shallow water equations, J. Comput. Phys. 208 (2005) 206–227.

[16] Y. Xing, C.W. Shu, High order well-balanced finite volume WENO schemes and discontinuous Galerkin methods for a class of hyperbolic systems with source terms, J. Comput. Phys. 214 (2006) 567–598.
[17] Y. Xing, X. Zhang, C.W. Shu, Positivity-preserving high order well-balanced discontinuous Galerkin methods for the shallow water equations, Adv. Water Resour. 33 (2010) 1476–1493.
[18] S.B. Yoon, C.H. Lim, L. Choi, Dispersion-correction finite difference model for simulation of transoceanic tsunamis, Terr. Atmos. Ocean. Sci. 18 (1) (2007) 31–53.
[19] M. Yuan, S.H. Song, A nonoscillatory finite volume method for 2D shallow water Equations on two-dimensional unstructured meshes, J. Numer. Methods Comput. Appl. 29 (1) (2008) 49–55.
[20] J.G. Zhou, D.M. Causon, C.G. Mingham, D.M. Ingram, The surface gradient method for the treatment of source terms in the shallow-water equations, J. Comput. Phys. 168 (2001) 1–25.
[21] J.S. Wang, H.G. Ni, Y.S. He, Finite-difference TVD scheme for computation of dam-break problems, J. Hydraul. Eng. 126 (4) (2000) 253–262.
[22] H.R. Vosoughifar, A. Dolatshah, S.K.S. Shokouhi, Discretization of multidimensional mathematical equations of dam break phenomena using a novel approach of finite volume method, J. Appl. Math. 2013 (2013) 1–12.
[23] Q.C. Zeng, Silt sedimentation and relevant engineering problem–an example of natural cybernetics, in: Proceedings of the Third International Congress on Industrial and Applied Mathematics, ICIAM95 held in Hamburg, Akademie Verlag, 1995, pp. 463–487.
[24] J. Zhu, Q.C. Zeng, D.J. Guo, Z. Liu, Optimal control problems related to the navigation channel engineering, Sci. China E 40 (1) (1997) 82–88.
[25] Z.D. Luo, J. Zhu, Q.C. Zeng, Z.H. Xie, Mixed finite element methods for shallow water equations including current and silt sedimentation (I): The Time continuous case, Appl. Math. Mech. 25 (1) (2004) 80–92.
[26] Z.D. Luo, J. Zhu, Q.C. Zeng, Z.H. Xie, Mixed finite element methods for shallow water equations including current and silt sedimentation (II): The discrete-case alone characteristics, Appl. Math. Mech. 25 (2) (2004) 186–201.
[27] G.S. Li, H.L. Wang, H.P. Liao, Simulation on seasonal transport variations and mechanisms of suspended sediment discharged from the Yellow River to the Bohai Sea, J. Geogr. Sci. 20 (6) (2010) 923–937.
[28] H.X. Zhang, A non-oscillatory and non-free parameter dissipation difference scheme, Acta Aerodyn. Sin. 6 (2) (1988) 143–165.
[29] T. Chung, Computational Fluid Dynamics, Cambridge University Press, Cambridge, 2002.
[30] R.X. Liu, C.W. Shu, Several New Methods for Computational Fluid Mechanics (in Chinese), Science Press, Beijing, 2003.